Ab Initio Electronic and Optical Properties of the $N - V^-$ Center in Diamond

Faruque M. Hossain,[1,*] Marcus W. Doherty,[1] Hugh F. Wilson,[2] and Lloyd C. L. Hollenberg[1]

[1]*Quantum Communications Victoria, School of Physics, University of Melbourne, Victoria 3010, Australia*

[2]*Ab initio Nanoscience Group, Chemistry Department, University of California–Davis, Davis, California 95616, USA*

(Received 17 September 2008; published 25 November 2008)

Despite tremendous activity in employing the $N - V^-$ center in a host of quantum technology applications, the electronic and optical properties of the system are still not theoretically well understood. We have conducted density functional theory calculations of the $N - V^-$ system which show convergence at the $3 \times 3 \times 3$ supercell level and for the first time produce a quantitatively accurate picture of the optical transition energy, excited-state lifetime, and optical polarization anisotropy taking into account all possible transitions within all contributing energy bands. These calculations were augmented by a group theoretical analysis, in sum providing a new *ab initio* understanding of this important solid-state quantum system.

DOI: 10.1103/PhysRevLett.101.226403 PACS numbers: 71.15.Mb, 31.15.ae, 31.15.ag, 71.55.−i

The negatively charged nitrogen-vacancy center ($N - V^-$) in diamond is the system of choice in many quantum technology applications, including quantum key distribution [1,2], implementation as a qubit [3], and as a sensitive magnetometer [4,5]. The center has been demonstrated to possess the highly desirable properties of single-photon generation [6,7], long-lived coherence [8], spin-spin coupling [9–11], electromagnetically induced transparency [12], and entanglement in small ensembles [13]. Empirically, the center's electronic, optical, and spin properties are consistently and extensively documented [14]. All of these achievements are at odds with the fact that, at an *ab initio* level, the $N - V$ center is not theoretically well understood. In this Letter, we report large scale *ab initio* density functional theory (DFT) calculations of the $N - V^-$ system which, for the first time, produce a consistent and quantitatively accurate picture of its optical properties (transition energy, excited-state lifetime, and optical polarization anisotropy). Augmented by a group theoretical (GT) analysis, these results provide new understanding of this important system.

Thus far in the literature, the predominant theoretical methods [15–20] applied to the center have been numerical calculations using either DFT or GT arguments based upon symmetry adapted molecular orbitals (MOs). Each approach has achieved varying degrees of success: GT provides a qualitative understanding of the electronic and spin structure, while DFT is a framework for numerical evaluation of the optical transition energies and excited-state lifetimes. However, to date, there has been no reported DFT calculation of the $N - V^-$ optical properties incorporating all possible direct transitions across the defect bands. Presumably, this is the reason why only qualitative agreement with experiment has been previously obtained. In order to provide an *ab initio* level understanding of the $N - V^-$ system, we conducted large supercell DFT calculations, including all contributing defect band transitions, of the center's optical properties. With excellent agreement with experiment, we use these results to infer modifications of the existing MO models. Subsequently, we show that a GT analysis using the modified MOs produces a picture consistent with the DFT calculations and experiment.

Experimental studies have established that the $N - V$ center is a defect site of trigonal (C_{3v}) symmetry which consists of a substitutional nitrogen atom adjacent to a carbon vacancy. Under optical excitation, the center exhibits a strong zero-phonon line at 1.945 eV (637 nm) [21] with an excited-state lifetime of 11.6 ns [22]. Observations of the center's electron spin resonance signal have revealed that the states involved in the transition are the spin triplet $^3A_2$ ground and ^3E excited states, implying that the center has integer spin ($S = 1$) and an even number of electrons. A six-electron model, in which the neutral $N - V$ center is assumed to have acquired an additional electron to form a negatively charged ($N - V^-$) center, has been generally accepted.

The MOs and state configurations of the $N - V^-$ center have been developed theoretically by Lenef and Rand [15] and in the pioneering early work of Loubser and van Wyk [20]. The symmetry adapted single electron MOs were constructed using linear combinations of one sp^3 nitrogen orbital (s_N) and three sp^3 carbon orbitals (s_1, s_2, and s_3) neighboring the vacancy. Two A_1 and two E symmetric MOs (labeled u, v and e_x, e_y, respectively) were identified. By applying symmetry and charge overlap considerations, the MOs were ordered energetically in each model as u, v, e_x, and e_y. Applying the Pauli exclusion principle and Hund's rules, the ground state configuration was identified as $u^2v^2e_xe_y$ and the degenerate excited-state configurations were identified as $u^2ve_x^2e_y$ and $u^2ve_xe_y^2$.

Our DFT methods were first applied to determine the MOs and energy levels of $N - V^-$ by calculating the center's spin-polarized band structure and orbital isosurfaces. Ultrasoft pseudopotentials were used with a plane-wave basis set cutoff energy of 300 eV (22 Ry) in the process of geometry optimization using the Broyden-

Fletcher-Goldfarb-Shanno quasi-Newton scheme [23], which preserves the symmetry of the defects. The electronic and optical properties were calculated using norm-conserving pseudopotentials with a basis set cutoff energy of 700 eV (52 Ry). The Perdrew-Burke-Enzerhof [24] form of the generalized gradient approximation was used for the exchange-correlation energy functional. 64-atom ($2 \times 2 \times 2$) and 216-atom ($3 \times 3 \times 3$) cubic supercells with side lengths $2a_0$ and $3a_0$, respectively, were used in the calculation. The 216-atom supercell has a significantly smaller defect concentration of 0.93% than the 64-atom: 3.13%. The k-point samplings for the $2 \times 2 \times 2$ and $3 \times 3 \times 3$ supercells were ($6 \times 6 \times 6$) and ($3 \times 3 \times 3$), respectively, according to the Monkhorst-Pack method, which generates 108 and 14 k points, respectively, in the irreducible Brillouin zone (BZ).

The calculated Kohn-Sham eigenstates (energy bands) in the band structure near the band gap are illustrated in Fig. 1(a). The $2 \times 2 \times 2$ supercell model displayed highly dispersive bands across the BZ due to defect-defect interactions, whereas only flat bands are observed in the $3 \times 3 \times 3$ supercell model. The spin-polarized calculation for

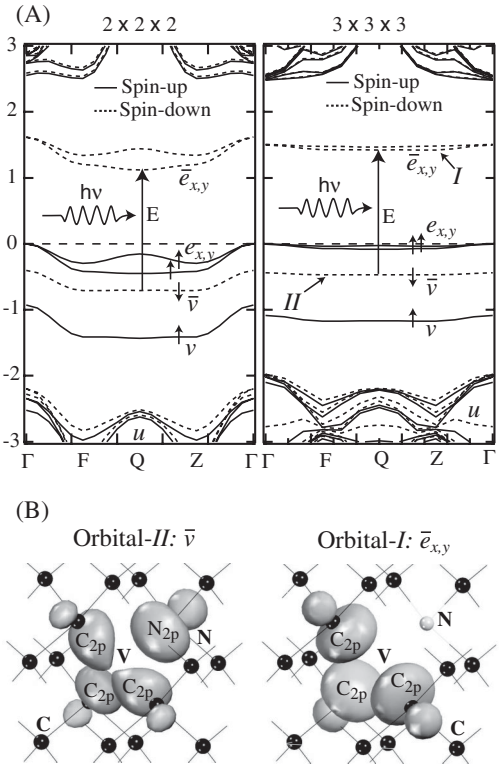

FIG. 1. (a) The spin-polarized ($S = 1$, $m_s = 1$) energy band structure for the $N - V^-$ center in diamond for a $2 \times 2 \times 2$ (left panel) and a $3 \times 3 \times 3$ (right panel) supercell (overbar denoting down spin). The dashed line at zero energy represents the Fermi level. The fractional coordinates of the k points in the Brillouin zone are $\Gamma(0, 0, 0)$, $F(0, 1/2, 0)$, $Q(0, 1/2, 1/2)$, and $Z(0, 0, 1/2)$. (b) Orbital isosurfaces of the $\bar{v}$ (highest occupied molecular orbital) and $\bar{e}_{x,y}$ (lowest unoccupied molecular orbital) electron orbitals.

($S = 1$, $m_s = 1$) generated three up-spin and three down-spin states inside the band gap. The two lowest energy occupied states possess A_1 symmetry and are merged with the valence band. The next four higher occupied states (one down-spin and three up-spin) are below the Fermi level. The lowest two of the four possess A_1 symmetry, and the higher two possess E symmetry. The two unoccupied antibonding states (down-spin) transform as E. Consequently, the calculations have reproduced the expected symmetry and ordering of the single electron states. The ground state spin configuration was confirmed to be $u\bar{u}v\bar{v}e_x e_y$ (overbar denoting down spin), using the integrated spin density. The band structure also confirms that the center's zero-phonon line transition (indicated by the arrow labeled "E") occurs between the occupied $\bar{v}$ and unoccupied $\bar{e}_{x,y}$ states.

The contributions of each atomic orbital to the MOs were assessed by producing volumetric visualizations of the electron density isosurfaces for each of the calculated single electron states. As expected, the visualizations of the collective $e_{x,y}$ MOs and the v MO in Fig. 1(b) clearly indicate that the $e_{x,y}$ MOs contain just contributions from three carbon orbitals and the v MO contains contributions from both nitrogen and three carbon orbitals. However, differing with Lenef and Rand [15], the calculated v MO contains a significant contribution from the nitrogen orbital, and the u MO is simply a nitrogen orbital. Reflecting these observations, the modified orthonormal MOs we propose are

$$\begin{aligned} u &= s_N, \qquad v = (s_1 + s_2 + s_3 - 3\beta s_N)/\sqrt{3}S_1, \\ e_x &= (2s_3 - s_1 - s_2)/\sqrt{3}S_2, \qquad e_y = (s_1 - s_2)/S_2, \end{aligned} \tag{1}$$

where $S_1 = \sqrt{1 + 2\alpha - 3\beta^2}$, $S_2 = \sqrt{2 - 2\alpha}$, $\alpha = \langle s_1 | s_2 \rangle$, and $\beta = \langle s_3 | u \rangle$ are normalization constants. Since our modified MOs possess the same symmetry properties and energy ordering as those of the previous models [15,20], the ground state and the doubly degenerate excited-state configurations are unchanged.

Applying the electric dipole approximation, the optical properties of the center were determined by evaluating the center's dielectric function $\epsilon(\omega) = \epsilon_1(\omega) + i\epsilon_2(\omega)$, which describes the linear response of the system to an electromagnetic wave. In particular, the imaginary component $\epsilon_2(\omega)$ is directly related to the absorption properties [25,26] of the center and was used to extract the center's optical transition energies. Within our DFT calculations, we determined $\epsilon_2(\omega)$ by evaluating the momentum operator matrix elements for all initial and final k points and applying Fermi's golden rule.

For each supercell, $\epsilon_2(\omega)$ was evaluated for the field polarization directions $N - V$, $N - Ci$, and $V - Ci$ [depicted schematically in Fig. 2(b)], and the results are shown in Fig. 2(a). The $2 \times 2 \times 2$ supercell $\epsilon_2(\omega)$ results along all three directions are dominated by three major peaks (P_1, P_2, and P_3) with the most dominant located at

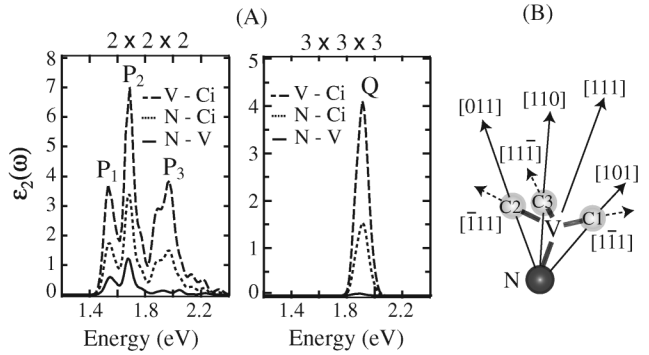

FIG. 2. (a) The frequency-dependent imaginary part of the dielectric function $\epsilon_2(\omega)$ evaluated for the electric field polarization directions: $N-V$ ([111]), $N-Ci$ ($i=1,2,3$) ([011], [101], and [110]), and $V-Ci$ ([$\bar{1}$11], [1$\bar{1}$1], and [11$\bar{1}$]). (b) Schematic of a $N-V$ center and relevant crystallographic directions.

P_2 (1.69 eV). The generation of such multiple structures is due to the considerable band dispersion in the $2\times2\times2$ supercell, as previously discussed in Fig. 1(a). The $3\times3\times3$ supercell results, in all directions, converge to a single peak at Q (1.912 eV), which is in excellent agreement with the experimentally observed 1.945 eV transition energy. This sharp peak originates from the less dispersive energy bands of the $3\times3\times3$ supercell [as seen in Fig. 1(a)], demonstrating that the volume is large enough to capture the physics of the center. The calculated momentum operator matrix elements were also used to evaluate the lifetime of the $3E$ excited state to be 13.1 ns ($3\times3\times3$ supercell), which also agrees well with experiment. The calculated transition energies and lifetimes are tabulated in Table I for comparison with previously reported experimental observations and theoretical results.

In order to facilitate the comparison of GT results with the DFT calculations and experiment, the normalized dielectric function $\hat{\epsilon}_2(\omega)$ was determined by GT arguments by expressing $\epsilon_2(\omega)$ in terms of the electric dipole operator $\hat{\mathbf{D}}$ and directly evaluating the transition dipole moments $\mathbf{D}$ using our proposed MOs. Near the ${}^3A\rightarrow{}^3E$ transition frequency ω_0, $\hat{\epsilon}_2(\omega)$ becomes

$$\hat{\epsilon}_2(\omega)=\frac{\epsilon_2(\omega)}{\max_{\mathbf{u}}[\epsilon_2(\omega)]}=\frac{(\mathbf{D}_{e_x}\cdot\mathbf{u})^2+(\mathbf{D}_{e_y}\cdot\mathbf{u})^2}{\max_{\mathbf{u}}[(\mathbf{D}_{e_x}\cdot\mathbf{u})^2+(\mathbf{D}_{e_y}\cdot\mathbf{u})^2]}, \quad (2)$$

TABLE I. Comparison of optical transition energies and excited-state lifetimes calculated using DFT methods with experimental data and other theoretical results.

	Transition energy (eV)	Radiative lifetime (ns)
$2\times2\times2$	1.69	17.6
$3\times3\times3$	1.912	13.1
Theory [16]	1.77	20
Theory [19]	1.867	...
Experiment	1.945 [21]	11.6 [22]

where $\mathbf{u}$ is the unit polarization vector of the incident photon, $\mathbf{D}_{e_x}=\langle{}^3A_2|\hat{\mathbf{D}}|{}^3E_x\rangle$ and $\mathbf{D}_{e_y}=\langle{}^3A_2|\hat{\mathbf{D}}|{}^3E_y\rangle$ are the transition dipole moments, $|{}^3A_2\rangle$ is the ground state, and $|{}^3E_x\rangle$ and $|{}^3E_y\rangle$ are the degenerate excited states.

Defining the local coordinate system (X,Y,Z) of the center such that the Z and X axes are directed along the [111] and [1$\bar{1}$0] crystal axes, respectively, the evaluation of the transition dipole moments can be simplified by using symmetry arguments. Given the choice of coordinate system, the Z component of the dipole operator will transform as A_1; hence, the Z components of the dipole moments are necessarily zero, since $A_2\otimes A_1\otimes E=E$, which does not contain the completely symmetric representation A_1 [27]. This conclusion agrees with the observations of strain-dependent optical measurements [21].

The remaining components of the dipole moments may be simplified by expressing the dipole operator in terms of the individual electron position operators $\hat{\mathbf{D}}=-e\sum_i^6\hat{\mathbf{r}}_i$ [27]. For such a sum of single electron operators, the matrix elements between the corresponding antisymmeterized spin-orbital states can be simplified to expressions involving just single electron states [27]: $\mathbf{D}_{e_x}=-e\langle v|\hat{\mathbf{r}}|e_x\rangle$ and $\mathbf{D}_{e_y}=-e\langle v|\hat{\mathbf{r}}|e_y\rangle$. The X and Y components of the single electron dipole operator transform as the x and y rows of the E representation, respectively. Therefore, given that the general basis element for the A_1 representation formed from the direct product $E\otimes E$ is $\frac{1}{2}\times(\psi_x\phi_x+\psi_y\phi_y)$, where $\{\psi_x,\psi_y\}$ and $\{\phi_x,\phi_y\}$ are the bases for the respective E representations [27], we conclude that the only nonzero dipole moment components are $\mathbf{D}_{e_x}=-e\langle v|\hat{\mathbf{X}}|e_x\rangle$ and $\mathbf{D}_{e_y}=-e\langle v|\hat{\mathbf{Y}}|e_y\rangle$. The magnitude of the dipole moments can be expressed in terms of atomic orbital parameters of the center by introducing the definitions of the MOs (1), exploiting the symmetry properties of the orbitals, and using the vector operator condition $P_R\hat{\mathbf{r}}P_R^{-1}=\mathbf{R}\hat{\mathbf{r}}$, where P_R and $\mathbf{R}$ are, respectively, the state and coordinate matrix representations of the element R of the C_{3v} group. The resulting dipole magnitudes are $|\mathbf{D}_{e_x}|=|\mathbf{D}_{e_y}|=D=e(r_{11}-3\beta r_{N1}+r_{21})/S_1S_2$, where $r_{ij}=|\langle s_i|\hat{\mathbf{r}}|s_j\rangle|$.

The dipole moment orientations are purely dependent on our choice of coordinate directions in the plane perpendicular to the center's symmetry axis. The symmetry of the center implies that there is no single preferred choice and that there are a number of distinct moment orientations which can be generated by applying each of the symmetry operations of the C_{3v} group to the above dipole orientations. Since each moment orientation will occur equally in the steady state interaction of the electromagnetic field with the $N-V$ center, all distinct moment orientations must be averaged over when $\epsilon_2(\omega)$ is evaluated. Adopting polar notation $\mathbf{D}_i=D(\cos\phi_i\hat{\mathbf{X}}+\sin\phi_i\hat{\mathbf{Y}})$, where $\hat{\mathbf{X}}$ and $\hat{\mathbf{Y}}$ are the unit coordinate vectors, the sets of dipole moment orientations (in radians) for each transition are

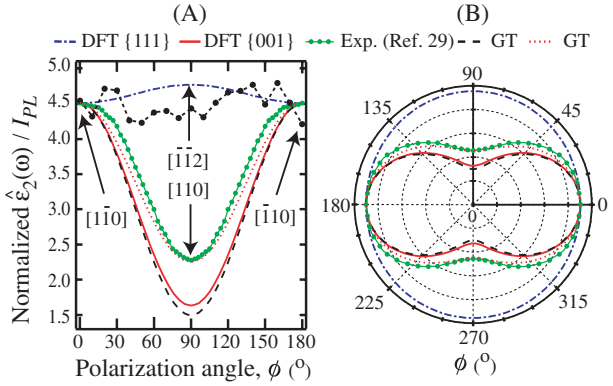

FIG. 3 (color online). (a) Normalized $\epsilon_2(\omega_0)$ (calculated) and photoluminescence intensity I_{PL} (experimental) versus the polarization angle ϕ in the {111} and {001} surfaces. (b) Normalized polar plot of the variation of $\epsilon_2(\omega_0)$ and I_{PL} in the {001} surfaces. Polarization along $\{1\bar{1}0\}$ corresponds to $\phi = 0°$, and data at ϕ and $\phi + 180$ are identical. (Black dashed-dotted line: Ref. [28]; blue dashed-dotted line: DFT; red solid line: DFT; green solid-dotted line: [29]; black dashed and red dotted lines: GT.)

$$\phi_{e_x} = \left[\frac{\pi}{3}, \pi, \frac{5\pi}{3}\right],$$
$$\phi_{e_y} = \left[\frac{\pi}{6}, \frac{\pi}{2}, \frac{5\pi}{6}, \frac{7\pi}{6}, \frac{3\pi}{2}, \frac{11\pi}{6}\right]. \quad (4)$$

We calculated the variation of $\epsilon_2(\omega_0)$ for field polarizations in the {111} and {001} surfaces using DFT (for the $3 \times 3 \times 3$ supercell) and GT methods and compared the variation with the experimental observations of the photoluminescence intensity by Alegre *et al.* [28] ({111} plane) and Epstein *et al.* [29] ({001} plane). The comparison of the normalized data sets for the variation of the polarization angle ϕ in each plane is depicted in Fig. 3(a). In the {111} plane, the GT data remain constant, and the DFT data oscillate only slightly about the GT constant magnitude. No significant difference can be concluded between our theoretical data and the experimental data of Alegre *et al.* [28], which seem to also fluctuate about a constant magnitude. In the {001} plane, the DFT and GT data again compare well, with only a small difference of $\approx 6\%$ present at $\phi = 90°, 270°$. Our theoretical data display a greater polarization variation than that observed in the experimental data of Epstein *et al.* [29] [depicted in Fig. 3(b)]. The variation of the DFT data can be quantified by the ratio $\epsilon_2(\omega_0, \phi = 0°)/\epsilon_2(\omega_0, \phi = 90°) = 2.76$, whereas the variation ratio reported by Epstein *et al.* is ≈ 2. This difference may be due to an anisotropic background luminescence or crystal strain present in the experiment. We found that if the electric field polarization was instead in a plane inclined by 10° from the {001} plane, toward the center's symmetry axis, the GT results [also plotted in Fig. 3(b)] are consistent with the data.

In conclusion, we have presented DFT calculation results which have for the first time accurately reproduced the zero-phonon line transition energy, excited-state lifetime, and polarization anisotropy of the $N - V^-$ center. The successful DFT calculations were used to infer changes to the symmetry adapted MOs of existing theoretical models. GT arguments were applied to the modified MOs to independently calculate the anisotropy of the center's dielectric function. Both methods of producing the dielectric function agreed excellently with each other and with previously reported experimental observations.

This project was supported by Quantum Communications Victoria, which is funded by the Victorian Government's Science, Technology and Innovation initiative, the Australian Research Council (Project No. DP0770715), and the International Science Linkages program.

*fhossain@unimelb.edu.au

[1] C. H. Bennett *et al.*, J. Cryptology **5**, 3 (1992).
[2] A. Beveratos *et al.*, Phys. Rev. Lett. **89**, 187901 (2002).
[3] M. V. Gurudev Dutt *et al.*, Science **316**, 1312 (2007); L. Childress *et al.*, Science **314**, 281 (2006).
[4] C. L. Degen, Appl. Phys. Lett. **92**, 243111 (2008); J. M. Taylor *et al.*, Nature Phys. **4**, 810 (2008).
[5] J. R. Maze *et al.*, Nature (London) **455**, 644 (2008); G. Balasubramanian *et al.*, Nature (London) **455**, 648 (2008).
[6] C. Kurtsiefer *et al.*, Phys. Rev. Lett. **85**, 290 (2000).
[7] R. Brouri *et al.*, Opt. Lett. **25**, 1294 (2000).
[8] F. Jelezko *et al.*, Phys. Rev. Lett. **92**, 076401 (2004).
[9] F. Jelezko *et al.*, Phys. Rev. Lett. **93**, 130501 (2004).
[10] T. Gaebel *et al.*, Nature Phys. **2**, 408 (2006).
[11] R. Hanson *et al.*, Phys. Rev. Lett. **97**, 087601 (2006); Science **320**, 352 (2008).
[12] C. Santori *et al.*, Phys. Rev. Lett. **97**, 247401 (2006).
[13] C. Santori *et al.*, Opt. Express **14**, 7986 (2006).
[14] Ph Tamarat *et al.*, New J. Phys. **10**, 045004 (2008).
[15] A. Lenef and S. C. Rand, Phys. Rev. B **53**, 13 441 (1996).
[16] J. P. Goss *et al.*, Phys. Rev. Lett. **77**, 3041 (1996).
[17] N. B. Manson, J. P. Harrison, and M. J. Sellars, Phys. Rev. B **74**, 104303 (2006).
[18] A. Gali, M. Fyta, and E. Kaxiras, Phys. Rev. B **77**, 155206 (2008).
[19] J. A. Larsson and P. Delaney, Phys. Rev. B **77**, 165201 (2008).
[20] J. H. N. Loubser and J. A. van Wyk, Rep. Prog. Phys. **41**, 1201 (1978).
[21] G. Davies and M. F. Hamer, Proc. R. Soc. A **348**, 285 (1976).
[22] A. Gruber *et al.*, Science **276**, 2012 (1997).
[23] B. G. Pfrommer *et al.*, J. Comput. Phys. **131**, 233 (1997).
[24] J. P. Perdew, K. Burke, and M. Ernzerhof, Phys. Rev. Lett. **77**, 3865 (1996).
[25] P. Palacios *et al.*, Phys. Rev. Lett. **101**, 046403 (2008).
[26] R. Asahi *et al.*, Science **293**, 269 (2001).
[27] M. Tinkham, *Group Theory and Quantum Mechanics* (McGraw-Hill, New York, 1964).
[28] T. P. M. Alegre *et al.*, Phys. Rev. B **76**, 165205 (2007).
[29] R. J. Epstein *et al.*, Nature Phys. **1**, 94 (2005).